Vol. 43, No. 3 (2021) 349-362, DOI: 10.24874/ti.984.10.20.01

Tribology in Industry

www.tribology.rs

RESEARCH

Effect of Dilution on Microstructure and Slurry Abrasive Wear Behaviour of Ni-Cr-Mo-W Coating on 304 Stainless Steel Deposited by Synergic Pulsed Gas Metal Arc Welding

A.P. Thummar[a,*], S.P. Wanare[a], V.D. Kalyankar[a]

[a]*Mechanical Engineering Department, S. V. National Institute of Technology, Surat, India*

Keywords:

Fluid catalytic cracking unit
Pulsed gas metal arc welding
Coating
Ni-Cr-Mo-W alloy
AISI 304 stainless steel
Dilution
Microstructure
Slurry abrasive wear

* Corresponding author:

Ankur P. Thummar
E-mail: apthummar89@gmail.com

Received: 14 October 2020
Revised: 23 November 2020
Accepted: 15 January 2021

A B S T R A C T

The paper aims to avoid premature failure of slide valve, flapper valve and slurry backflush system for fluid catalytic cracking unit due to slurry abrasive wear by depositing Ni-Cr-Mo-W alloy on 304 austenitic stainless steel using synergic pulsed gas metal arc welding. An average coating thickness was obtained in the range of 2.41 mm to 2.78 mm and dilution level varied from 17% to 26.74%. The microstructure revealed that hypoeutectic Ni-FCC dendrites and interdendritic region with MC, $M_{23}C_6$ and M_6C carbides were present. The formation of carbides was directly related to dilution level of the coating, since dilution level influenced the proportional amount of carbon and carbide forming alloying elements. Slurry abrasive wear resistance initially increased with an increase in dilution level up to 23.88% of dilution, later on it started to decrease due to reduction in solid solution alloying elements and carbide fraction. Slurry abrasive wear resistance of the coated surface was found up to 3.5 times higher than that of the substrate. The mechanism of abrasive wear under the operation of microcuttings, pits formation and ploughing with a little plastic deformation was witnessed on the worn-out surfaces.

1. INTRODUCTION

Austenitic stainless steels (ASSs) are extensively used material in petroleum refinery because of their excellent corrosion resistance [1]. AISI 304 ASS is well known corrosion resistant material used in petrochemical industries. Slide valve [2], flapper valve [3] and slurry backflush system [4] of fluid catalytic cracking unit (FCCU) in petroleum refinery are largely exposed to highly corrosive and abrasive wear environment. These components have frequent premature failure due to abrasive working environment of slurry oil, which consists of dispersed cracking catalyst particles and metal containing heavy gas oil. According to primary hazard analysis by Rooney

et al. [5], slide valves are expected to fail once in a year and it incur an approximate economic loss of $65,000 per failure event, while flapper valves are expected to fail several times during a life time of the plant and incur an approximate economic loss of $200,000 per failure event, and a failure in slurry backflush system is expected to occur once during a life time of the plant, which incur an approximate economic loss of $650,000 per failure event. In order to improve the service life of such components, coating of advanced grade materials is a solution to avoid premature failure of these components [6].

Ni-based alloys have been popular for applications of wear and corrosion environment, because of their ability to accommodate large range of alloying elements compared to other alloys [7-8]. Ni-Cr-Mo-W alloy presents high strength even without heat treatment because of solid solution alloying elements Mo and W [9]. These elements are also strong carbide formers and provide good mechanical properties by the formation of hard phases like molybdenum carbide and tungsten carbide [10]. Graf and D'Oliveira [11] deposited Ni-Cr-Mo-W alloy on AISI 304L and AISI 1020 substrates using plasma transferred arc (PTA) deposition process. It was observed that the coating had superior corrosion and wear resistance at high temperature up to 600°C. Microstructure of PTA coated Ni-Cr-Mo-W alloy on ASS substrate was studied by Ferreira et al. [10], which revealed that the microstructure of the coating comprised of hypoeutectic Ni-FCC dendrites and interdendritic region with MC (Mo, W) and $M_{23}C_6$ (Cr) blocky carbides. Rivero et al. [9] stated that the wear resistance and hardness were influenced by two factors, solid solution strengthening and carbide fraction. Dilution level in coating affects proportional amount of solid solution alloying elements and carbide fraction. Further, the effect of dilution level on carbide fraction depends upon relative amount of elemental concentration in coating material and substrate. Dilution is the most important aspect of any weld overlay deposition process. Dilution significantly influences the microstructure of weld coating, which directly regulates wear characteristics and microhardness of weld coating [12].

The process like PTA is highly automated and cost effective for large scale production [13]. However, such automated processes become costly approach for some job specific small scale applications. Hence, cost effective manual based welding process like gas metal arc welding (GMAW) become appropriate solution due to its high productivity, flexibility, low economical cost and easy availability of the machine. Luchtenberg et al. [14] deposited duplex stainless steel coating on a mild steel plate using GMAW process and evaluated coating properties such as coating thickness, dilution level, microhardness, wear behaviour and microstructural aspects for different heat input. Frequent innovations in the technique have increased weld quality. Among them, the pulsed GMAW process has been popular in the welding industry due to its precise control over the thermal cycle and comparatively low heat input. Pal and Pal [15] stated that in pulsed GMAW process, more precisely controlled droplet metal transfer is obtained at low current intensity. D'Oliveira et al. [16] confirmed that pulsed current process provides finer structure, which is attributed to solidification kinetic involved with pulsed current process. The pulsed current causes an increase in nucleation rate, as dendrites arms rupture owing to the molten pool agitation. The higher nucleation rate during solidification leads to a higher growing rate of the structure. Higher undercooling takes place during pulsed current process due to the increased temperature gradient in the molten pool. Benoit et al. [17] have compared four arc welding processes used for coating; GMAW, pulsed GMAW, cold metal transfer (CMT) and tungsten inert gas (TIG) welding. The same level of residual stresses and the same size of heat affected zone (HAZ) in pulsed GMAW and CMT depositions was observed. Prabhu and Alwarsamy [18] studied the effect of process parameters on ferrite number in coating deposition of 317L ASS by pulsed GMAW process. It was found that the welding speed and welding current had more influence on ferrite number than other process parameters. Suresha et al. [19] effectively deposited Ni-Cr-Mo-W alloy on 316L ASS using GMAW and studied microstructure and abrasive wear behaviour of the coating. The specific wear rate of the coating was found 41% lower than that of the substrate. The worn-out surface indicated abrasive wear mechanism under the operation of microcutting and microploughing.

Investigations on Ni-Cr-Mo-W coating have been addressed in previous studies. However, literature on abrasive wear behaviour of Ni-Cr-Mo-W alloy coating is scarce. Hence, this article aims to evaluate the effect of dilution on microstructure, microhardness, slurry abrasive wear behaviour and morphology of the worn-out surfaces of Ni-Cr-Mo-W coating, which may be beneficial to avoid premature failure of slide valve, flapper valve and slurry backflush system for FCCU.

2. MATERIALS AND METHODS

The welding process test chart is shown in Fig. 1. The subsequent contents in this section explain its each method in detail.

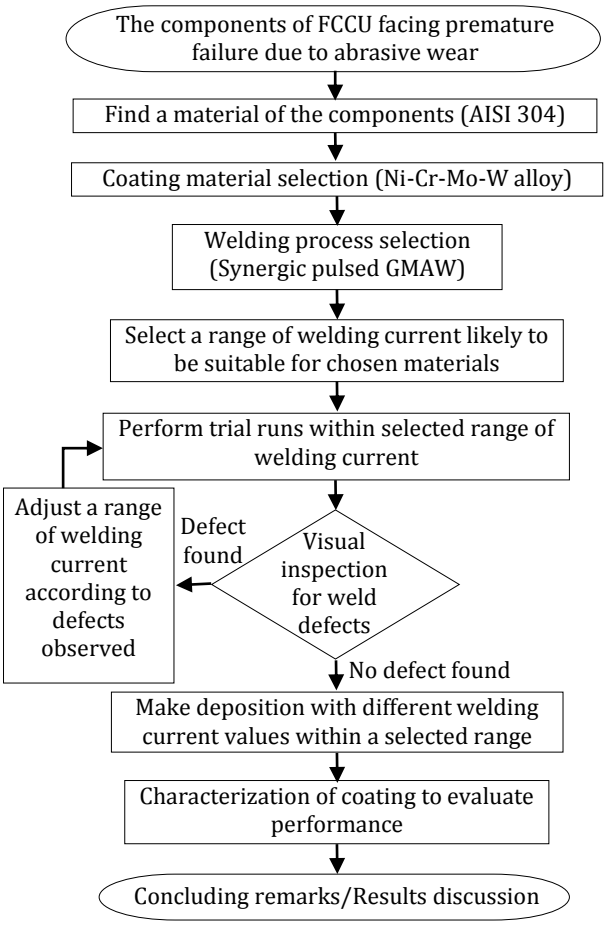

Fig. 1. Welding process test chart

In the present work, cold rolled 304 ASS plate was used as a substrate material with specimen size of 200 mm x 150 mm x12 mm. Table 1 gives chemical composition of 304 ASS.

Ni-Cr-Mo-W alloy was selected as coating material based on properties obtained from the past data. This alloy is available as a solid metal wire of 1.2 mm diameter in the market. Chemical composition of the Ni-Cr-Mo-W alloy wire is given in Table 2. Fronius TPS 320i welding machine was used for coating deposition.

Before deposition on the specimens, large number of trial runs were performed on the cleaned substrate surface to finalise the range of process parameters and to observe the coating behaviour as well. During the trial runs, no crack was observed on the coating even without preheating of substrate material, unlike many previous researches with different coating material. This is attributed to good weldability of the Ni-Cr-Mo-W alloy and almost similar coefficient of thermal expansion of the substrate material and the Ni-Cr-Mo-W alloy.

During trial experiment, lack of fusion and insufficient bonding between the coating and substrate were observed below 130 A mean pulse current, whereas above mean pulse current of 180 A more spatters and burn through were witnessed. From the trial experiments and material suitability, the range of process parameters were finalised, which are given in Table 3. Here, it should be noted that voltage and wire feed rate are adjusted automatically with a change in welding current, since synergic mode of welding is selected.

Before coating, the specimens were tacked on the thick plate through welding to minimize distortion. These specimens were immediately kept for sand bath for slow cooling and to avoid formation of oxide layer.

In order to get sufficient wear strength, minimum coating thickness should be ensured throughout the overlaid surface. To measure average coating thickness of specimens, cross sectional profiles of coated specimens are captured and measurements of coating thickness are taken with AutoCAD software as shown in Fig. 2. The average of a coating thickness at various point across coating is considered as average coating thickness.

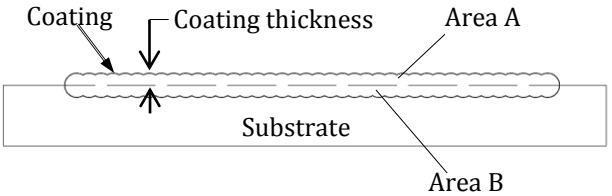

Fig. 2. Standard procedure for measurement of dilution based on area

Table 1. Chemical composition of 304 ASS

Element	C	Cr	Ni	Mn	Si	P	Fe
wt.%	0.06-0.08	18-20	8-11	2 max.	0.75-1	0.04-0.05	Bal.

Table 2. Chemical composition of Ni-Cr-Mo-W alloy

Element	C	Cr	Mo	W	Co	Fe	Ni
wt.%	0.02	14.63	16.19	3.44	0.23	6.11	57.65

Table 3. Process parameters for experiment

Specimen	Mean pulse current (A)	Voltage (V)	Wire feed rate (m/min)
S1	130	20.6	5.1
S2	140	21.0	5.5
S3	150	21.3	5.9
S4	160	21.7	6.3
S5	170	22.0	6.7
S6	180	22.4	7.1
Shielding gas: 80% Ar + 20% CO_2 **Gas flow rate:** 10 lit/min **Interpass temperature:** 250°C			

In order to obtain strong metallurgical bond between the substrate and Ni-Cr-Mo-W alloy, mixing of the materials at the interface is necessary. Due to this mixing, some substrate material rises in coating layer, known as dilution. Dilution causes variation in chemical composition, microstructure and eventually affects mechanical performance of coating such as hardness, wear and corrosion resistance. Here, dilution measurement is performed on the basis of area measurement. In this method, area of substrate metal in weld zone (Area *B*) and total weld zone area (Area *A+B*) is measured at the cross section of the coating specimen as shown in Fig. 2. Similar approach has been employed in literature [12, 20]. Dilution percentage is calculated by using equation (1).

$$\text{Dilution}(\%) = \frac{B}{(A+B)} \times 100 \quad (1)$$

The microstructural analysis of the selected coated specimens was carried out through scanning electron microscopy (SEM). X-ray diffraction (XRD) analysis was carried out on the coating surface using X-Ray diffractometer with Cu Kα (1.5405 Å) radiation and maximum diffraction angle (θ) of 90° to identify various phases formed in the coating. Inorganic crystal structure database (ICSD) was used for phase identification from the diffraction patterns, which has been similarly reported by Adesina et al. [21]. ICSD comprises crystallographic database for fully identified inorganic structure complemented with scientific journals and other relevant sources. The carbide fraction was measured using ImageJ software.

Microhardness of the Ni-Cr-Mo-W deposition on 304 ASS was measured through Vickers microhardness tester with an applied load of 0.5 kg for 10 second. Indentations were taken on the cross section from the substrate towards the coating surface. Distance between two indentations was maintained as 0.5 mm.

Slurry abrasive wear test is most suitable to evaluate and to compare the wear behaviour on surfaces of slide valve, flapper valve and slurry backflush system of FCCU under corresponding working environment. Hence, slurry abrasive wear test was performed as per ASTM G105 standard with Ducom, India make slurry abrasive wear test rig to reveal wear resistance of applied coating. The parameters used during wear tests are given in Table 4.

Table 4. Wear test parameters [22]

Test parameters	Values
Specimen size	(25.4 ± 0.8 mm) x (57.2 ± 0.8 mm) x (6.4 to 15.9 mm)
Test load	222 N
Test time	1000 revolutions
RPM	245 rpm
Sand	-50/ +70 mesh

Fig. 3 shows schematic of slurry abrasive wear test as per ASTM G105 standard. According to ASTM G105 standard, wear test should be performed with three rubber wheel of shore hardness of 50, 60 and 70 with hardness tolerance of ± 2.0. Specimens are weighted to accuracy of 0.0001 gram before and after wear test on each rubber wheel. Calculated weight loss is obtained based on 60 shore hardness rubber wheel from least square line as per procedure given in ASTM G105 standard. Weight measurement was done with Shimadzu make weighing balance having accuracy of 0.0001 gram.

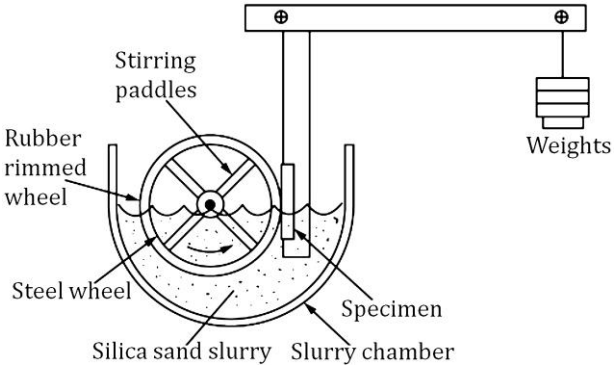

Fig. 3. Schematic of slurry abrasive wear test apparatus [22]

In order to correlate the obtained wear characteristics, in-depth study of worn-out surface was also performed with SEM. The Ni-Cr-Mo-W coated specimens which showed lowest and highest slurry abrasive wear resistance were selected to examine the worn-out surface morphology.

3. RESULTS AND DISCUSSION

3.1 Analysis on average coating thickness

The average coating thickness values for different conditions can be found between 2.41 to 2.78 mm (Table 5). Average coating thickness increases with an increase in current intensity as shown in Fig. 4, following previous work [14]. In the case of synergic process, voltage and wire feed rate were adjusted automatically as mean pulse current was changed (Table 3). All other process parameters were kept constant. So, heat input was governed by voltage and mean pulse current increased along with an increase in rate of deposition volume.

At lower heat input level, coating thickness can be found less sensitive to change in heat input. On the other hand, at higher heat input level, coating thickness varies significantly with change in heat input (Fig. 4). According to literature, at lower mean pulse current level the increase in voltage decreases coating thickness by enlarging bead width and at higher mean pulse current the increase in voltage does not change coating thickness substantially due to various forces responsible for fluid flow mechanism [23]. Here, as heat input increases, wire feed rate also increases and thus volume of material deposited per second per unit length increases, provided welding speed is kept constant. Hence, a collective effect of the increase in wire feed rate and the increase in voltage cause almost constant coating thickness at lower heat input level, while the latter becomes negligible at higher heat input level and the former causes an increase in coating thickness.

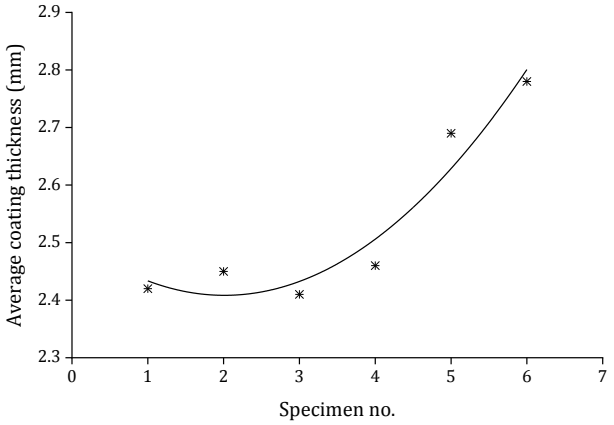

Fig. 4. Average coating thickness (Note: The higher the specimen no., the higher the heat input)

3.2 Analysis on weld dilution

Table 5 shows percentage dilution measurement for each specimen. Fig. 5 shows percentage dilution for different conditions. As expected, interaction with the substrate increased with an increase in weld heat input [21]. Further, it can be observed that dilution level for the coating is strongly dependent on weld heat input. Measured values of percentage dilution vary from 17% to 26.74% (Table 5). The higher interaction for coating on 304 ASS is a consequence of the lower thermal conductivity of the ASS [16].

Table 5. Measurement of percentage dilution and average coating thickness

Specimen	Average coating thickness (mm)	Area A (mm^2)	Area B (mm^2)	Dilution (%) $= \frac{B}{(A+B)} \times 100$
S1	2.42	270.4564	55.3622	17.00
S2	2.45	246.8109	80.2106	24.52
S3	2.41	252.9515	79.3408	23.88
S4	2.46	250.7508	88.2359	26.03
S5	2.68	267.5772	97.2161	26.65
S6	2.78	282.2412	103.0202	26.74

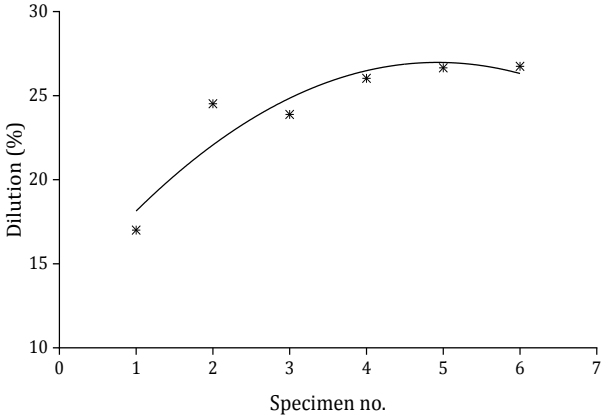

Fig. 5. Percentage dilution by area method (Note: The higher the specimen no., the higher the heat input)

3.3 Microstructural analysis

Fig. 6 shows the micrographs of interface between 304 ASS substrate and Ni-Cr-Mo-W alloy weld coating processed with 150 A mean pulse current (S3), which revealed the highest wear resistance during the test. The microstructure of the weld coating is complex and changes with distance from the interface. As revealed in Fig. 6(a), the microstructure exhibits an interface line followed by planer, columnar and dendritic or cellular region respectively. The interface between Ni-Cr-Mo-W alloy weld coating and 304 ASS substrate can be found sharp as clearly depicted from the micrograph. Fig. 6(b) shows that interface is a thin layer of fine grains near to the substrate. The formation of thin layer occurs because the substrate plays the role of nucleation site for heterogeneous nucleation and its cooling rate is high [8]. The growth of microstructure is controlled by the cooling rate and direction [24]. Therefore, dendrites grow in the direction of the coating thickness. Further, the interface can be found free from delamination and microcracks.

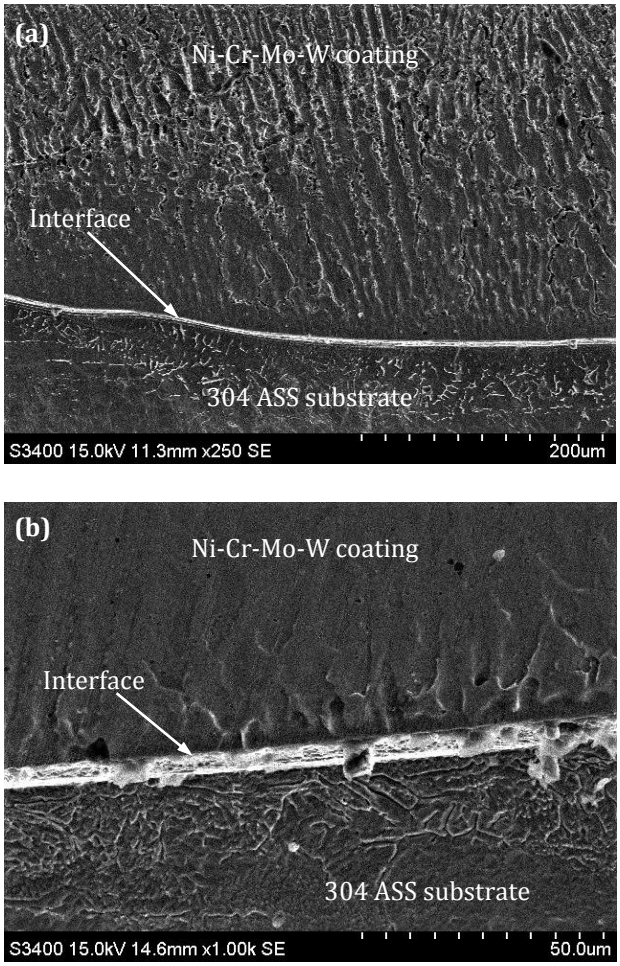

Fig. 6. SEM micrographs at interface region of Ni-Cr-Mo-W coating on 304 ASS processed with 150 A mean pulse current (S3)

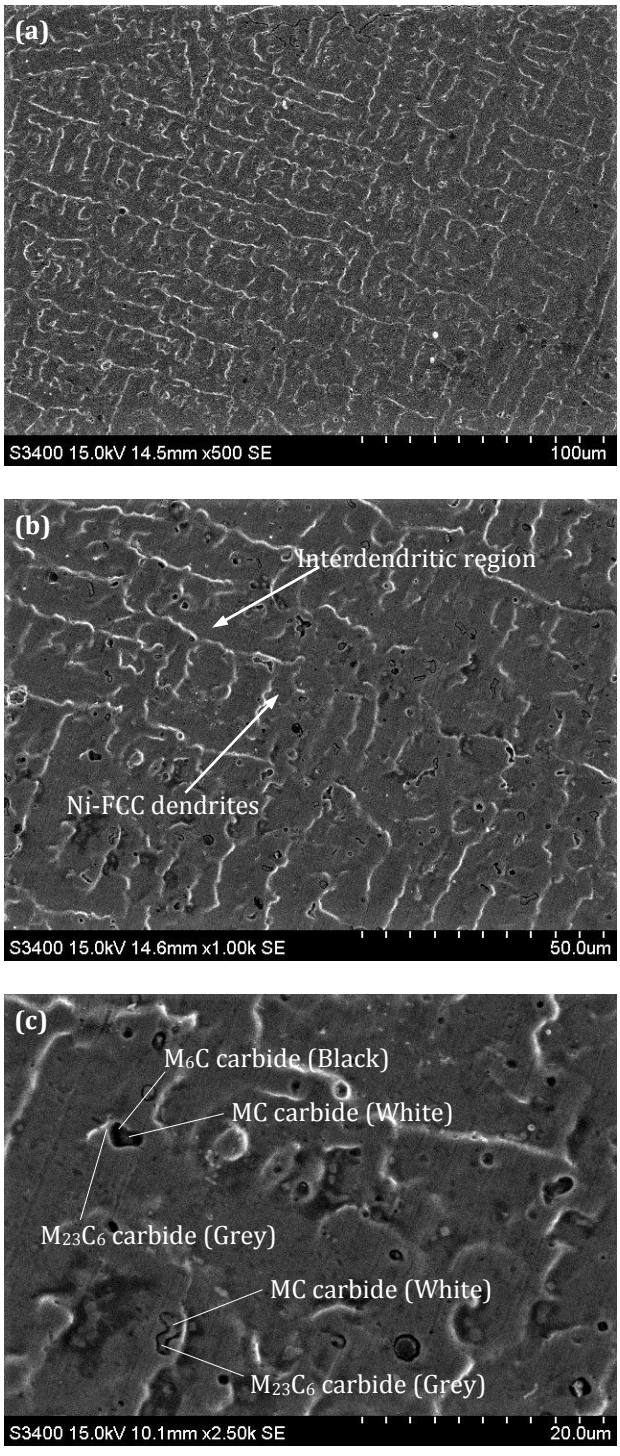

Fig. 7. SEM micrograph of Ni-Cr-Mo-W coating on 304 ASS processed with 150 A mean pulse current (S3)

The microstructural analysis of the specimens exhibited lowest (S1) and highest (S3) wear resistance for slurry abrasion was performed through SEM to correlate their wear resistance with the microstructure. The SEM images in Fig. 7 and Fig. 8 are representing the upper most portion in cross section of coated specimens. SEM micrographs of the coated specimen processed with 150 A mean pulse current (S3), which revealed the highest wear resistance during the test are shown in Fig. 7. The microstructure revealed hypoeutectic Ni-FCC dendrites and interdendritic region with carbides, which was also reported by Graf and D'Oliveira [11]. XRD patterns shown in Fig. 9 also reveals the presence of [Ni, Fe]-FCC phase and different carbides on coatings. Table 6 contains the crystallographic data from ICSD used to identify phases in the XRD pattern. The diffraction peaks of Ni-FCC solid solution moved a little towards small angle compared with the XRD standard diffraction card in both the cases of Specimen S1 and Specimen S3. The reason behind aforementioned phenomenon is an internal stress generated in the crystal structure due to substitution of elements of Fe in Ni-FCC solution, since both the elements have different atom size [25]. But the difference in atom size is minor, otherwise such substitution is not possible.

Small blocky structures distributed in the micrograph can be observed in Fig. 7(b) and Fig. 7(c). Two types of blocky structures can be found in the microstructure. The first type comprises a block of two carbides in contrast of white and grey colours that are MC (where M is Mo or W) and $M_{23}C_6$ (where M is Cr) type carbides respectively [26]. The second type comprises a block of three carbides in contrast of black and grey colours around white colour that are M_6C (where M is Fe, Ni, Mo or W), $M_{23}C_6$ and MC type carbides respectively [26]. These carbides significantly enhance the hardness and slurry abrasive wear resistance of the coating. The XRD pattern also confirms the presence of these carbides (Fig. 9). While the XRD pattern for the specimen processed with 130 A mean pulse current (S1) reveals the presence of all above said phases in the structure, except M_6C carbide (Fig. 9). The factor responsible to the formation of M_6C type carbide in the coated specimen processed with 150 A mean pulse current (S3) is higher concentration of C and Si owing to higher dilution level. It is reported that the M_6C type carbide doesn't form at low C content [9], while Si stabilises and promotes the formation of M_6C type carbide [27]. The M_6C carbide is also known as η-carbide and it may have stoichiometry form of Fe_3Mo_3C, Fe_3W_3C, Fe_2Mo_4C, Ni_3Mo_3C, Ni_3W_3C, Ni_2Mo_4C or Ni_2W_4C [28].

The XRD patterns revealed that M_7C_3 (where M is Cr) type carbide is not present in the microstructure (Fig. 9), because high proportional amount of Mo supressed the formation of M_7C_3 type carbide and promoted the formation of $M_{23}C_6$ type carbide [29].

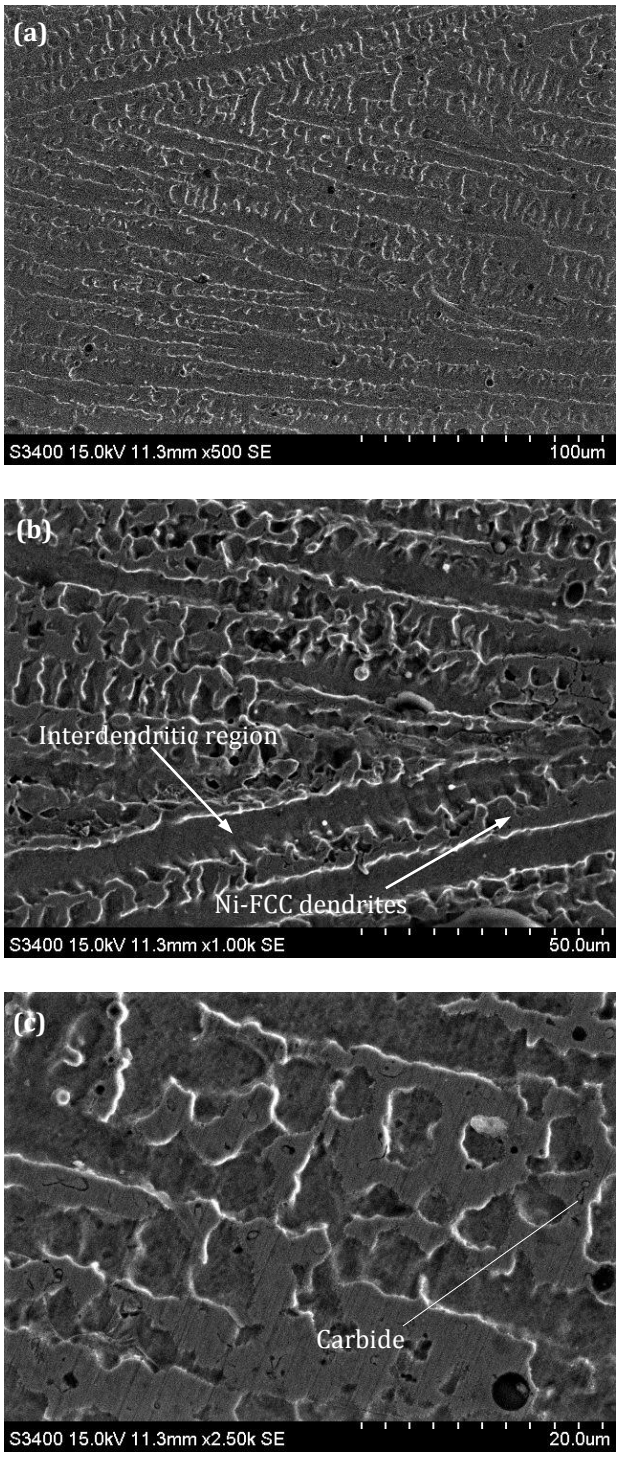

Fig. 8. SEM micrograph of Ni-Cr-Mo-W coating on 304 ASS processed with 130 A mean pulse current (S1)

Fig. 8 shows SEM micrographs of the coated specimen processed with 130 A mean pulse current (S1), which revealed the highest wear loss during slurry abrasive wear test. In this specimen also, the microstructure revealed hypoeutectic Ni-FCC dendrites and interdendritic region, but Ni-FCC dendrites can be observed smaller than the former case (S3) and hence dendrites are finer.

The peaks of Ni-FCC in the pattern for specimen processed with 130 A mean pulse current (S1) (Flex width of 0.64, 0.55 and 0.27 respectively) can be found broader than those in the pattern for specimen processed with 150 A mean pulse current (S3) (Flex width of 0.59, 0.54 and 0.26 respectively). It indicates that the former has finer grain structure of Ni-FCC than the latter [25].

From Fig. 9, it can be observed that the diffraction peaks of Ni-FCC solid solution for the specimen processed with 130 A mean pulse current (S1) is situated a little towards small angle compared with the specimen processed with 150 A mean pulse current (S3) due to different strain in the crystal structure generated through chemical heterogeneity. This takes place due to solution of higher concentration of Mo and W in the former case compared with the latter case [30]. The higher the concentration of such elements, the higher the chemical heterogeneity and thus higher the strain in structure. An approximate proportional amount of any element in the coating can be given by equation (2). With an increase in dilution level the proportional amount of carbon in the coating increases, since the wire material itself has lower amount of C than the substrate material (Table 1 and Table 2). The lower the dilution level, the lower the proportional amount of carbon in the solution, causes less carbide fraction formation at higher concentration of Mo and W. Hence, more free elements of Mo and W without any composition are available.

$$\%X\text{ in coating} = [\%X\text{ in wire} \times (1 - \frac{Dilution(\%)}{100})] + [\%X\text{ in substrate} \times \frac{Dilution(\%)}{100}] \quad (2)$$

Table 6. ICSD data used for identification of the phases by XRD analysis

Phase	Structure type	SG HMS*	Formula	ICSD collection code
γ FCC-(Ni, Fe)	Face centered cubic	225 Fm-3m	Ni	646087 [31]
M_6C	Face centered cubic	227 Fd-3m	Fe_3W_3C	76760 [32]
			Fe_3Mo_3C	617778 [33]
			Fe_2Mo_4C	76135 [28]
			Ni_3W_3C	166884 [32]
			Ni_3Mo_3C	76134 [28]
			Ni_2Mo_4C	76137 [28]
			Ni_2W_4C	618587 [33]
MC	Face centered cubic	225 Fm-3m	WC	162417 [34]
			MoC	43523 [35]
$M_{23}C_6$	Face centered cubic	225 Fm-3m	$Cr_{23}C_6$	191594 [36]

* Hermann–Mauguin symbol for space group

Furthermore, the carbide fractions on the specimen processed with 150 A mean pulse current (S3) and the specimen processed with 130 A mean pulse current (S1) were found 2.19% and 0.94% respectively. Hence, it can be confirmed that formation of carbides is strongly depended upon dilution level.

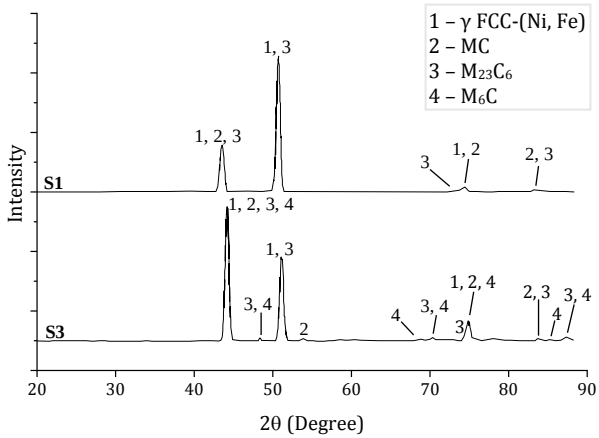

Fig. 9. XRD patterns for coatings processed with 130 A mean pulse current (S1) and 150 A mean pulse current (S3)

3.4 Analysis of microhardness

Vickers hardness cross-section profiles of coating for different specimens are shown in Fig. 10. It can be seen that all coatings have higher hardness than the substrate. The microhardness profiles show increasing trend from substrate to top surface of coating. The distribution of the obtained microhardness values of the developed coatings is not uniform. This may have resulted from the presence of complex phases of [Ni, Fe]-FCC, MC, $M_{23}C_6$ and M_6C in the microstructure (section 3.3), which have different hardness. The authors reported similar larger fluctuations in hardness for Ni-based coatings [24, 37]. At the substrate, microhardness can be found approximately 195 $HV_{0.5}$, it stands for microhardness of 304 ASS. Overall, highest microhardness on the coating is 235 $HV_{0.5}$ and average microhardness on the coating is 220 $HV_{0.5}$.

There is no clear trend within the investigated range of heat input for coating region. Rivero et al. [9] also reported similar observation for Ni-Cr-Mo-W alloy coating on GGG 40 ductile iron, the substrate material having higher proportional amounts of C than the coating material. Generally, HAZ of substrate undergoes heat treatment during deposition that causes nucleation and growth of austenite resulting in reduction of dislocation number and work hardening, which directly affect hardness of the structure. Fig. 10 shows that microhardness in HAZ (the portion of substrate adjacent to interface) is different for various heat input, since heat input strongly influence nucleation and grain growth.

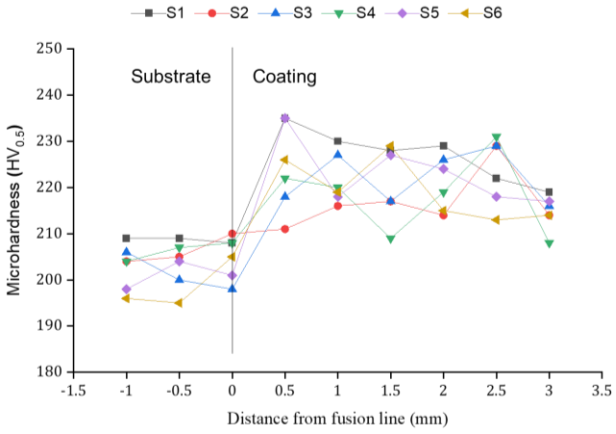

Fig. 10. Vickers hardness cross-section profiles (Note: The higher the specimen no., the higher the heat input)

3.5 Analysis on slurry abrasive wear behaviour

The wear loss for different process conditions is presented in the plot given in Fig. 11. Wear resistance of the coated surfaces was found up to 3.5 times higher than that of the substrate material. The lower wear loss of Ni-Cr-Mo-W coated surface is attributed to the presence of hard phases of in coating and solid solution alloying, which protect the coating layer against abrasive working environment of slurry oil and improves wear strength of the coating. The hard phases include chromium carbides, molybdenum carbides and tungsten carbides, the explanation about the same has been given in section 3.3.

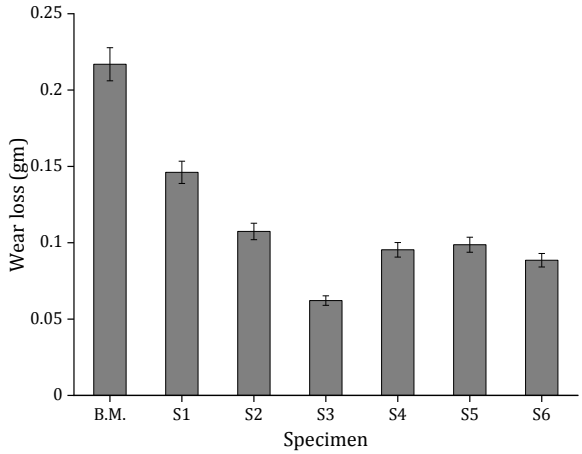

Fig. 11. Slurry abrasive wear loss for different conditions (Note: The higher the specimen no., the higher the heat input)

It can be observed that initially wear loss decreases with an increase in dilution level, after particular dilution level (23.88%), wear loss started to increase with dilution level (Fig. 11). Such behaviour can be attributed to changes in carbide fraction with an increase in dilution level. Here, as explain in section 3.3, the specimen processed with 150 A mean pulse current (S3) has a higher carbide fractions than the specimen processed with 130 A mean pulse current (S1), hence the former has shown lower wear loss compared to the latter (Fig. 11). As dilution level increased, the proportional amount of solid solution alloying elements reduced (equation 2) and carbide fraction increased significantly until a certain dilution level as a consequence of higher carbon diluted from the substrate. Later on, in spite of addition of an even higher amount of diluted carbon from the substrate, the reduction of carbide forming alloy elements limited the further increase in carbide fraction.

Similar phenomenon was reported in the literature for Ni-Cr-Mo-W alloy coating on GGG 40 iron (the substrate material having higher proportional amounts of C than the coating material) using laser cladding [9]. Although, hardness influences wear performance of the material, any straight forward effect of hardness cannot be observed, following previous work [37].

3.6 Analysis of worn-out surface morphology

Fig. 12 and Fig. 13 indicate worn-out surfaces of the selected coating surfaces of the specimen with the lowest (S3) and the highest (S1) wear loss during slurry abrasive wear test respectively.

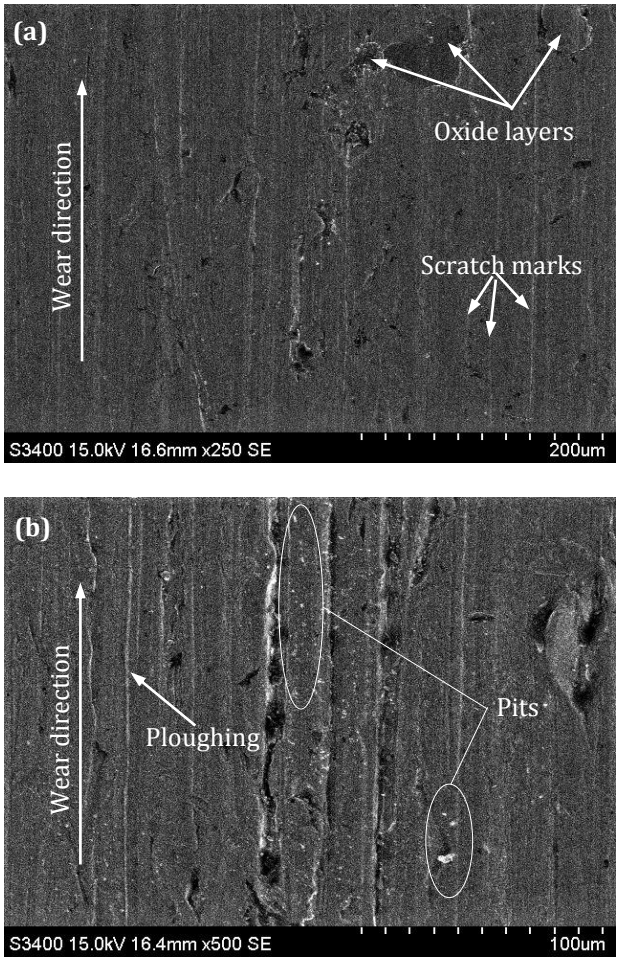

Fig. 12. SEM images of worn-out surface processed with 150 A mean pulse current (S3)

The images showed almost flat surface without delamination of the coating. The microcuttings in the form of scratch marks were observed in the magnified images. The microcuttings were formed due to the high stress contact of abrasive

silica particle on the surface [38]. Ploughing can also be observed on the worn-out surfaces owing to silica particles and detached metal particles' role in subsequent wear loss [8]. The microcutting and ploughing are common phenomenon for wear under the abrasive environment [7, 39-40]. Therefore, main wear mechanism was abrasive wear.

Pits were present on the worn-out surface processed with 150 A mean pulse current (S3) due to detaching of hard phases like carbides from the coating surface as shown in Fig. 12(b). The cloud like structures can be observed in Fig. 12(a), it is considered to be the oxide layers formed due to compaction of wear debris particles that are completely or partially oxidized [8].

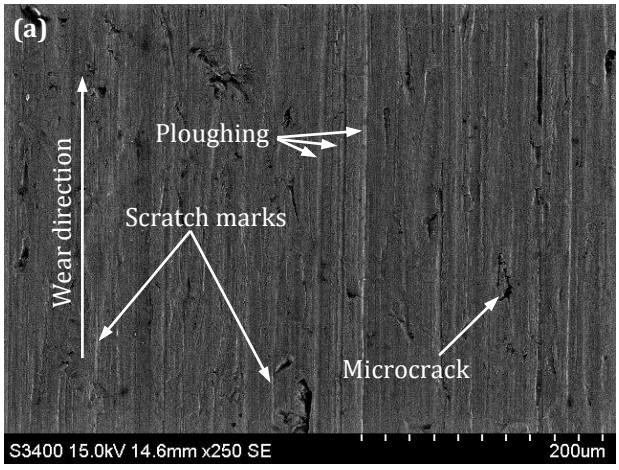

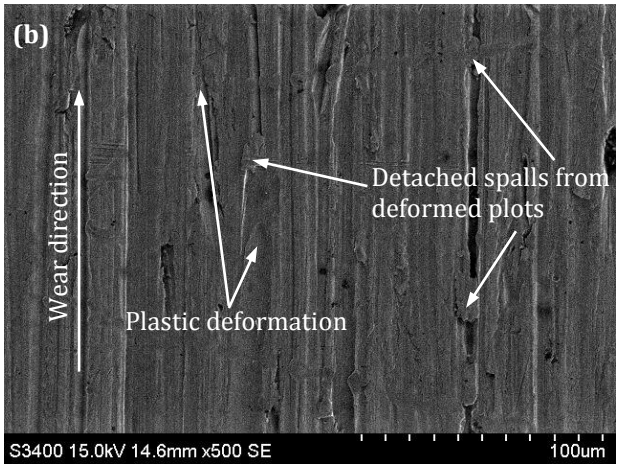

Fig. 13. SEM images of worn-out surface processed with 130 A mean pulse current (S1)

The surface morphology of the worn-out surface processed with 130 A mean pulse current (S1) consisted of plastic deformation besides scratch marks. Some of the detached spalls from deformed plots can also be observed in Fig. 13(b). The microcracks are also observed within deformed plot as shown in Fig. 13(a). The worn-out surface of the latter can be found smoother and pits were not present on the worn-out surfaces unlike the former case, it may be due to lower amount of carbides that are present in the coating.

With careful investigation of the images, it can be found that for the coating surface processed with 130 A mean pulse current (S1), relatively wider grooves induced with bulk removal of the coating material compared to the coating surface processed with 150 A mean pulse current (S3). The above-mentioned observation justifies the higher wear loss for the specimen processed with 130 A mean pulse current (S1).

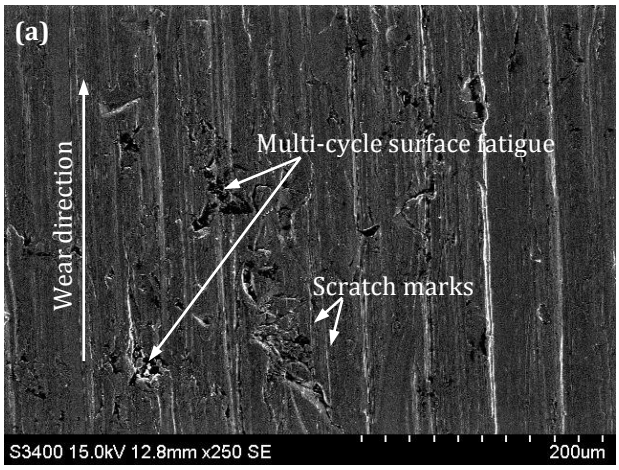

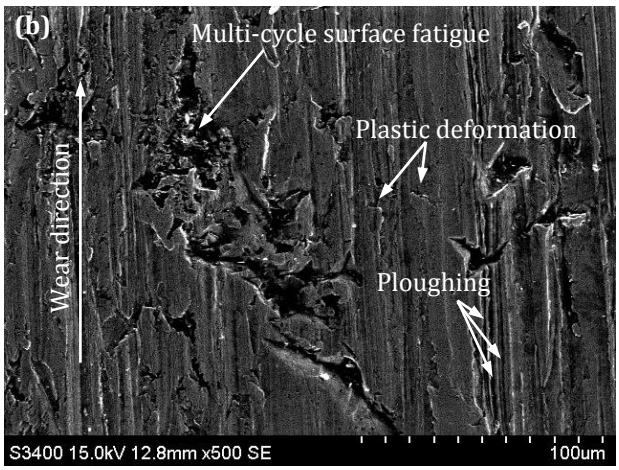

Fig. 14. SEM images of worn-out surface of base metal

Fig. 14 indicates worn-out surface of base metal. The intensified scratches and ploughing operations can be found in the form of much wider and deeper grooves. This may occur due

to lower hardness and absence of any hard phases in structure. A multi-cycle surface fatigue was also witnessed on the surface. It took place due to blasting of large size debris on the soft surface [39], which were produced due to deep cutting. It made material to chip off from the surface. The occurrence of aforementioned phenomena resulted in largest mass loss of the specimen (Fig. 11).

Hence, the coated surface with process parameters corresponding to the specimen processed with 150 A mean pulse current (S3) is best suitable for the components exposed to slurry abrasive wear environment.

4. CONCLUSIONS

The Ni-Cr-Mo-W alloy coating was successfully deposited on 304 ASS using synergic pulsed GMAW process at different conditions of process parameters. A good bonding between the substrate metal and coating material was obtained without any surface cracks or lack of adhesion. Surface characteristics of the coating such as average coating thickness and dilution, microstructure of coated specimens, microhardness profile, slurry abrasive wear behaviour and morphology of worn-out surface were analysed. Based on the obtained results, following conclusions can be drawn:

- An average coating thickness was obtained in the range of 2.41 mm to 2.78 mm and dilution level varied from 17% to 26.74%.
- The microstructure of Ni-Cr-Mo-W coating revealed hypoeutectic Ni-FCC dendrites and interdendritic region with MC, $M_{23}C_6$ and M_6C carbides.
- The formation of carbides was strongly depended on dilution level of the coating.
- Slurry abrasive wear resistance initially increased with dilution level, after 23.88% of dilution, it started to decrease as a consequence of reduction in solid solution alloying elements and carbide fraction with an increase in dilution level. Slurry abrasive wear resistance of the Ni-Cr-Mo-W coating was up to 3.5 times higher than that of the substrate material.
- The wear mechanism was a dominant abrasive wear in the form of microcuttings, pits formation and ploughing with a little plastic deformation for the coated surfaces.

The overall observation shows that the coating of Ni-Cr-Mo-W alloy on 304 ASS by synergic pulsed GMAW with controlled process parameters can provide an effective solution to avoid premature failure of slide valve, flapper valve and slurry backflush system for FCCU with a cost effective manual welding process.

REFERENCES

[1] P. Varghese, E. Vetrivendan, M.K. Dash, S. Ningshen, M. Kamaraj, U.K. Mudali, *Weld overlay coating of Inconel 617M on type 316L stainless steel by cold metal transfer process*, Surface and Coatings Technology, vol. 357, pp. 1004-1013, 2019, doi: 10.1016/j.surfcoat.2018.10.073

[2] L.A. Lattanzio, A. Green, M.R. Wojtowicz, I.G. Horn, *Early prediction and detection of slide valve sticking in petrochemical plants or refineries*, Patent US10678272, 2020.

[3] P. Czarnecki, *Check valve*, Patent US10487955, 2019.

[4] Q. Sun, J. Wu, L. Dong, Z. Zhang, J. Liu, J. Yue, F. Yan, *Gas-liquid-solid three-phase slurry bed industrial reactor capable of achieving continuous operation*, Patent US10363535, 2019.

[5] J.J. Rooney, J.H. Turner, J.S. Arendt, *A preliminary hazards analysis of a fluid catalytic cracking unit complex*, Journal of Loss Prevention in the Process Industries, vol. 1, iss. 2, pp. 96-103, 1988, doi: 10.1016/0950-4230(88)80019-6

[6] D.D. Deshmukh, V.D. Kalyankar, *Deposition characteristics of multitrack overlay by plasma transferred arc welding on SS316L with Co-Cr based alloy – Influence of process parameters*, High Temperature Materials and Processes, vol. 38, pp. 248-263, 2019, doi: 10.1515/htmp-2018-0046

[7] E. Zdravecka, M. Ondac, J. Tkacova, *Tribological behavior of thermally sprayed Coatings with different chemical composition and modified by remelting*, Tribology in Industry, vol. 41, no. 4, pp. 463-470, 2019, doi: 10.24874/ti.2019.41.04.01

[8] C. Guoqing, F. Xuesong, W. Yanhui, L. Shan, Z. Wenlong, *Microstructure and wear properties of nickel-based surfacing deposited by plasma transferred arc welding*, Surface and Coatings Technology, vol. 228, pp. S276–S282, 2013, doi: 10.1016/j.surfcoat.2012.05.125

[9] L.E.H.S. Rivero, A. Pizzatto, M.F. Teixeira, A. Rabelo, T. Falcade, A. Scheid, *Effect of laser power and substrate on the Hastelloy C276TM coatings features deposited by laser cladding*, Materials Research, vol. 23, no. 2, pp. 1-11, 2020, doi: 10.1590/1980-5373-mr-2020-0067

[10] L.D.S. Ferreira, K. Graf, A. Scheid, *Microstructure and properties of nickel-based C276 alloy coatings by PTA on AISI 316L and API 5L X70 steel substrates*, Materials Research, vol. 18, no. 1, pp. 212-221, 2015, doi: 10.1590/1516-1439.332914

[11] K. Graf, A.S.C.M. D'Oliveira, *Microstructural stability and wear performance of a Ni based alloy PTA coating*, in Proceedings of the 17th International Congress of Mechanical Engineering – COBEM, 10–14 November, 2003, Sao Paulo, Sao Paulo: COBEM, pp. 156–161.

[12] S. Saroj, C.K. Sahoo, M. Masanta, *Microstructure and mechanical performance of TiC-Inconel 825 composite coating deposited on AISI 304 steel by TIG cladding process*, Journal of Materials Processing Technology, vol. 249, pp.490-501, 2017, doi: 10.1016/j.jmatprotec.2017.06.042

[13] D.D. Deshmukh, V.D. Kalyankar, *Recent status of overlay by plasma transferred arc welding technique*, International Journal of Materials and Product Technology, vol. 56, no. 1/2, pp. 23–83, 2018, doi: 10.1504/IJMPT.2018.089118

[14] P. Luchtenberg, P.T. de Campos, P. Soares, C.A.H. Laurindo, O. Maranho, R.D. Torres, *Effect of welding energy on the corrosion and tribological properties of duplex stainless steel weld overlay deposited by GMAW/CMT process*, Surface and Coatings Technology, vol. 375, pp. 688-693, 2019, doi: 10.1016/j.surfcoat.2019.07.072

[15] K. Pal, S.K. Pal, *Effect of pulse parameters on weld quality in pulsed gas metal arc welding: a review*, Journal of Materials Engineering and Performance, vol. 20, no. 6, pp. 918-931, 2011, doi: 10.1007/s11665-010-9717-y

[16] A.S.C.M. D'Oliveira, R. Paredes, R. Santos, *Pulsed current plasma transferred arc hardfacing*, Journal of Materials Processing Technology, vol. 171, iss. 2, pp. 167-174, 2006, doi: 10.1016/j.jmatprotec.2005.02.269

[17] A. Benoit, P. Paillard, T. Baudin, V. Klosek, J.B. Mottin, *Comparison of four arc welding processes used for aluminium alloy cladding*, Science and Technology of Welding and Joining, vol. 20, iss. 1, pp. 75-81, 2015, doi: 10.1179/1362171814Y.0000000257

[18] R. Prabhu, T. Alwarsamy, *Effect of process parameters on ferrite number in cladding of 317L stainless steel by pulsed MIG welding*, Journal of Mechanical Science and Technology, vol. 31, no. 3, pp. 1341-1347, 2017, doi: 10.1007/s12206-017-0234-x

[19] B. Suresha, S.G. Channabasavanna, N.S. Shanmugam, *Microstructure and abrasive wear behaviour of nickel based hardfacing stainless steel deposited by gas metal arc welding*, Applied Mechanics and Materials, vol. 895, pp. 278-283, 2019, doi: 10.4028/www.scientific.net/AMM.895.278

[20] P. Reinaldo, A.S.C.M. D'Oliveira, *NiCrSiB coatings deposited by plasma transferred arc on different steel substrates*, Journal of Materials Engineering and Performance, vol. 22, no. 2, pp. 590-597, 2013, doi: 10.1007/s11665-012-0271-7

[21] O.S. Adesina, B.A. Obadele, G.A. Farotade, D.A. Isadare, A.A. Adediran, P.P. Ikubanni, *Influence of phase composition and microstructure on corrosion behavior of laser based Ti–Co–Ni ternary coatings on Ti–6Al–4V alloy*, Journal of Alloys and Compounds, vol. 827, p. 154245, 2020, doi: 10.1016/j.jallcom.2020.154245

[22] ASTM G105-16, *Standard test method for conducting wet sand/rubber wheel abrasion tests*, 2016.

[23] M. Sen, M. Mukherjee, T.K. Pal, *Evaluation of correlations between DP-GMAW process parameters and bead geometry*, Welding Journal, vol. 94, no. 8, pp. 265s-279s, 2015.

[24] H.X. Hu, X.M. Guo, Y.G. Zheng, *Comparison of the cavitation erosion and slurry erosion behavior of cobalt-based and nickel-based coatings*, Wear, vol. 428, pp. 246-257, 2019, doi: 10.1016/j.wear.2019.03.022

[25] T. Ungar, *Microstructural parameters from X-ray diffraction peak broadening*, Scripta Materialia, vol. 51, iss. 8, pp. 777-781, 2004, doi:10.1016/j.scriptamat.2004.05.007

[26] X. Dong, X. Zhang, K. Du, Y. Zhou, T. Jin, H. Ye, *Microstructure of carbides at grain boundaries in nickel based superalloys,* Journal of Materials Science and Technology, vol. 28, iss. 11, pp. 1031-1038, 2012, doi: 10.1016/S1005-0302(12)60169-8

[27] L. Jiang, X.X. Ye, Z.Q. Wang, C. Yu, J.S. Dong, R. Xie, Z.J. Li, L. Yan, T.K. Sham, X.T. Zhou, A.M. Li, *The critical role of Si doping in enhancing the stability of M_6C carbides*, Journal of Alloys and Compounds, vol. 728, pp. 917-926, 2017, doi: 10.1016/j.jallcom.2017.09.042

[28] K. Kuo, *The formation of η carbides*, Acta Metallurgica, vol. 1, no. 3, pp. 301-304, 1953, doi: 10.1016/0001-6160(53)90103-5

[29] Q.Y. Hou, Z.Y. Huang, N. Shi, J.S. Gao, *Effects of molybdenum on the microstructure and wear resistance of nickel-based hardfacing alloys investigated using Rietveld method*, Journal of Materials Processing Technology, vol. 209, iss. 6, pp. 2767-2772, 2009, doi: 10.1016/j.jmatprotec.2008.06.025

[30] Q.Y. Wang, Y.F. Zhang, S.L. Bai, Z.D. Liu, *Microstructures, mechanical properties and corrosion resistance of Hastelloy C22 coating produced by laser cladding*, Journal of Alloys and Compounds, vol. 553, iss. 6, pp. 253-258, 2013, doi: 10.1016/j.jmatprotec.2008.06.025

[31] J. Bandyopadhyay, K.P. Gupta, *Low temperature lattice parameter of nickel and some nickel-cobalt alloys and Gruneisen parameter of nickel*, Cryogenics, vol. 17, iss. 6, pp. 345-347, 1977, doi: 10.1016/0011-2275(77)90130-8

[32] Y. Li, Y. Gao, Z. Fan, B. Xiao, Q. Yue, T. Min, S. Ma, *First-principles study on the stability and mechanical property of eta M_3W_3C (M = Fe, Co, Ni) compounds*, Physica B: Condensed Matter, vol. 405, no. 3, pp. 1011-1017, 2010, doi: 10.1016/j.physb.2009.10.045

[33] P. Ettmayer, R. Suchentrunk, *Uber die thermische stabilitat der eta-carbide*, Monatshefte fur Chemie, vol. 101, no. 4, pp. 1098-1103, 1970, doi: 10.1007/BF00908553

[34] D.V. Suetin, I.R. Shein, A.L. Ivanovskii, *Structural, electronic properties and stability of tungsten mono-and semi-carbides: A first principles investigation*, Journal of Physics and Chemistry of Solids, vol. 70, iss. 1, pp.64-71, 2009, doi: 10.1016/j.ceramint.2013.10.022

[35] E.V. Clougherty, K.H. Lothrop, J.A. Kafalas, *A new phase formed by high-pressure treatment: face-centred cubic molybdenum monocarbide*, Nature, vol. 191, p. 1194, 1961, doi: 10.1038/1911194a0

[36] Z.Q. Lv, F. Dong, Z.A. Zhou, G.F. Jin, S.H. Sun, W.T. Fu, *Structural properties, phase stability and theoretical hardness of $Cr_{23-x}M_xC_6$ (M= Mo, W; x= 0–3)*, Journal of Alloys and Compounds, vol. 607, pp. 207-214, 2014, doi: 10.1016/j.jallcom.2014.03.188

[37] A.M. Hebbale, M. Srinath, *Microstructural investigation of Ni based cladding developed on austenitic SS-304 through microwave irradiation*, Journal of Material Research and Technology, vol. 5, iss. 4, pp. 293–301, 2016, doi: 10.1016/j.jmrt.2016.01.002

[38] G.R. Piazzetta, L.E. Lagoeiro, I.F.R. Figueira, M.A.G. Rabelo, G. Pintaude, *Identification of abrasion regimes based on mechanisms of wear on the steel stylus used in the Cerchar abrasiveness test*, Wear, vol. 410-411, pp. 181-189, 2018, doi: 10.1016/j.wear.2018.07.009

[39] K. Ligier, J. Napiorkowski, M. Lemecha, *Effect of abrasive soil mass grain size on the steel wear process*, Tribology in Industry, vol. 42, no. 2, pp. 165-176, 2020, doi: 10.24874/ti.784.10.19.04

[40] A. Hernandez-Pena, E.A. Gallardo-Hernandez, L.I.F. Cabrera, M. Vite-Torres, *Study of the influence of abrasive particles on a journal bearing with a soft coating (Pb-Cu-Al) under boundary lubrication conditions*, Proceedings on Engineering Sciences, vol. 1, no. 1, pp. 347-356, 2019, doi: 10.24874/PES01.01.045